RSC Advances

PAPER

View Article Online
View Journal | View Issue

Cite this: *RSC Adv.*, 2021, **11**, 25955

Facile synthesis of copper selenides with different stoichiometric compositions and their thermoelectric performance at a low temperature range†

Longbin Li,[a] Yifang Zhao,[a] Chaosheng Shi,[a] Wei Zeng,*[a] Bing Liao,[b] Mingqiu Zhang[c] and Xiaoming Tao[d]

Received 15th June 2021
Accepted 14th July 2021

DOI: 10.1039/d1ra04626h

rsc.li/rsc-advances

Copper selenide is widely considered to be a promising candidate for high-performance flexible thermoelectrics; however, most of the reported *ZT* values of copper selenides are unsatisfactory at a relatively low temperature range. Herein, we utilized some wet chemical methods to synthesize a series of copper selenides. XRD, SEM and TEM characterizations revealed that CuSe, Cu_3Se_2 and $Cu_{2-x}Se$ were prepared successfully and possessed different morphologies and sizes. Based on the analysis of their thermoelectric properties, $Cu_{2-x}Se$ exhibited the highest Seebeck coefficient and lowest thermal conductivity among the three samples owing to its unique crystal structure. After being sintered at 400 °C under N_2 atmosphere, the electrical conductivity of $Cu_{2-x}Se$ enhanced considerable, resulting in a significant improvement of its *ZT* values from 0.096 to 0.458 at 30 to 150 °C. This result is remarkable for copper selenide-based thermoelectric materials at a relatively low temperature range, indicating its brilliant potential in the field of flexible thermoelectric devices.

Introduction

In recent years, wearable and implantable electronic devices have been receiving increasing attention and further development for their multiple applications in various fields relating to human bodies, such as cardiac pacemakers, cochlear implants, gastric stimulators, physiological sensors, smart watches, and smart glasses.[1] For the sake of extending the usage time of such devices effectively, researchers have proposed two main strategies: one is expanding the capacity of the power source used in the wearable devices, and the other is harvesting energy from the human body or the surrounding environment to fabricate the so-called self-powered devices.[2] For the second construction method, the flexible thermoelectric (FTE) materials are considered promising candidates that meet the requirement well. The advantages of FTE materials in manufacturing such self-powered devices include: (a) they can operate well within physiological temperatures,[3,4] and (b) their light weight allows the conformable attachment onto human skin or other organs to utilize the body heat maximally.[5,6] Thus, FTE materials are convinced to play an increasingly important role in self-powered devices in the near future, and relevant researches are flourishing.

Among the different types of inorganic thermoelectric (TE) materials, tellurides such as Bi_2Te_3 and PbTe are the most commonly studied and used nowadays.[7–9] However, these tellurides contain rare-earth and toxic elements, thus driving researchers to develop alternative economical and eco-friendly TE materials with satisfactory TE properties.[7] Compared with tellurium, selenium has a much higher earth abundance and is relatively less toxic. Hence, numerous selenides such as Cu_2Se,[10] SnSe,[11,12] PbSe,[13] In_4Se_3,[14] Ag_9GaSe_6,[15] and Cu_3SbSe_4 (ref. 16) have been introduced into TE application researches in recent years, and many of them have exhibited excellent TE performance. Cu_2Se or $Cu_{2-x}Se$ is one of the most remarkable selenides in TE researches due to its unique crystal structure. In the high-temperature β-phase of $Cu_{2-x}Se$, the Se atoms form a rigid crystalline sublattice while the copper ions are highly dispersed around the Se skeletons disorderly with liquid-like mobility.[10] Such crystalline structure corresponds to the ideal phonon-glass electron-crystal model for high-efficiency TE materials. Besides, numerous types of synthesis methods have been applied in building copper selenide-based TE materials,[17–30]

[a]*Guangdong Key Laboratory of Industrial Surfactant, Institute of Chemical Engineering, Guangdong Academy of Sciences, Guangzhou 510665, China. E-mail: zengwei@gdcri.com*

[b]*Guangdong Academy of Sciences, Guangzhou 510665, China*

[c]*Key Laboratory for Polymeric Composite and Functional Materials of Ministry of Education, GD HPPC Lab, School of Chemistry and Chemical Engineering, Sun Yat-Sen University, Guangzhou 510275, P. R. China*

[d]*Research Centre for Smart Wearable Systems, Institute of Textiles and Clothing, The Hong Kong Polytechnic University, Hong Kong*

† Electronic supplementary information (ESI) available. See DOI: 10.1039/d1ra04626h

some of which were even constructed as FTE devices.[25,26] The morphology and TE performance of these copper selenides differ from each other to a certain degree under different synthesis conditions. To date, the highest *ZT* value of copper selenide-based TE materials has reached as high as 2.7,[24] which is comparatively among the highest *ZT* values of all types of TE materials. However, many of the high *ZT* values of copper selenides are attained at very high temperatures, such as in the range of 800–1000 K. For FTE applications, it is usually supposed that the FTE devices should operate well near room temperature (RT) or at relatively low-temperature range. Nowadays, many of the reported *ZT* values of pure copper selenides are still less than 0.3 near RT.[30] Thus, the TE performance of copper selenides needs further improvement at the relatively low-temperature range.

In this study, we utilized facile wet chemical methods for the synthesis of a series of copper selenide nanomaterials. The as-prepared copper selenide samples were first characterized by XRD, SEM and TEM tests. The results show that copper selenides with different stoichiometric compositions such as CuSe, Cu_3Se_2 and $Cu_{2-x}Se$ were successfully obtained *via* separate synthetic processes, and they possessed different morphologies and particle sizes. Further, TE performance tests were conducted between 30 and 150 °C, and the $Cu_{2-x}Se$ sample exhibited the highest Seebeck coefficient and the lowest thermal conductivity values among the three samples. After being sintered at 400 °C under an N_2 atmosphere, the electrical conductivity of the $Cu_{2-x}Se$ sample significantly improved, and the highest *ZT* value reached about 0.46 at 150 °C, which is an impressive result for copper selenides at a relatively low temperature range.

Experimental section

Preparation of the copper selenides

Sample 1 (S1, CuSe): 0.33 g SeO_2 and 1.5 g $CuSO_4 \cdot 5H_2O$ were first dissolved in 50 mL DI water. Then, 1.26 g Na_2SO_3 was added to the solution and stirred for 5 min. Then, the mixture was poured into a 100 mL stainless steel autoclave and heated to 80 °C for 12 h. After the hydrothermal reaction was completed, the obtained precipitates were rinsed with DI water and ethanol, followed by drying at 60 °C.

Sample 2 (S2, Cu_3Se_2): 0.32 g Se and 1.26 g Na_2SO_3 were first mixed in 50 mL water and stirred for 1 h at 80 °C. After cooling down to RT, the mixture was filtered, and the supernatant was poured into a 50 mL solution containing 2 g $CuSO_4 \cdot 5H_2O$. Then, the mixture was further stirred at RT for 2 h. After the reaction finished, the precipitates were rinsed with DI water and ethanol and dried at 60 °C.

Sample 3 (S3, $Cu_{2-x}Se$): 0.33 g SeO_2 and 1.5 g $CuSO_4 \cdot 5H_2O$ were first dissolved in 50 mL DI water, and then 2.0 g sodium ascorbate was dissolved in 30 mL DI water. After all the chemicals were completely dissolved, the sodium ascorbate solution was poured into the SeO_2 and $CuSO_4$ mixture solution, and the mixed solution was kept stirring for 2 h at RT. The mixture was allowed to rest for a few hours after stirring, and then the precipitates were washed with DI water and ethanol successively, and finally dried at 60 °C.

Sample 4 (S4, s-$Cu_{2-x}Se$): S3 was placed into a tube furnace and sintered at 400 °C under an N_2 atmosphere for 1 h. The heating rate was 10 °C min^{-1}, and the N_2 was flowing during both the heating and cooling processes.

Characterization and measurements of the copper selenide samples

The crystal structure of the samples was characterized by X-ray diffractometry (XRD, Rigaku9000, Rigaku Corporation, Japan). The morphology of the as-prepared powders was examined by field emission scanning electron microscopy (FE-SEM, SU8220, Hitachi, Japan). Further structural and phase identification were performed by transmission electron microscopy and high-resolution transmission electron microscopy (TEM and HRTEM, Talos F200s, FEI, USA).

Seebeck coefficient and electrical conductivity of the samples were tested by Seebeck coefficient measurement (LSR-3, Linseis, Germany) at the range of 30 to 150 °C. The as-prepared powders were pressed into 1.3 cm wide disks for the test. The applied pressure was 10 MPa and lasted for 5 min. Thermal conductivity was directly measured by a thermal conductivity analyzer (TPS 2500S, Hot Disk, Sweden) at the range between 30 and 150 °C.

A temperature controller (TLTP-TEC2415D, TLT, China) was used to provide temperature difference, and an electrochemical workstation (CHI810D, Chenghua, China) was used to record and analyze the stimulated electric signals. The as-prepared powders were pressed into a 1.5 cm wide and 2.0 cm long rectangle-shaped bulk for the output voltage test, whereby the applied pressure was 10 MPa and lasted for 5 min.

Results and discussion

After being rinsed and dried, the as-prepared samples were characterized by XRD, and the results are shown in Fig. 1. Fig. 1(a) shows the XRD pattern of S1 (CuSe), and the red vertical

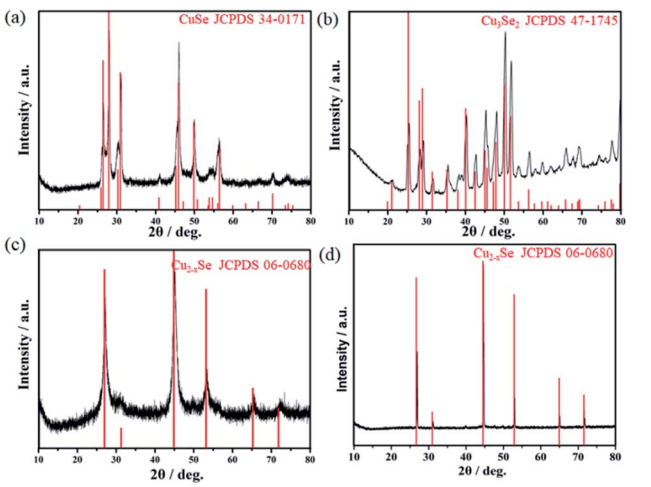

Fig. 1 XRD patterns of the as-synthesized samples S1–S4 (a–d).

lines reflect the standard diffraction peaks of mineral klockmannite CuSe (JCPDS card no. 34-0171). One can notice that the corresponding XRD peaks of CuSe tally with the standard peaks. Fig. 1(b) is the XRD pattern of S2 (Cu_3Se_2), and the standard diffraction peaks of mineral umangite Cu_3Se_2 (JCPDS card no. 47-1745) are also shown. Most of the corresponding XRD peaks can be identified as that of Cu_3Se_2, and the weak peak at about 39° probably belongs to Se (JCPDS card no. 27-0603). Fig. 1(c) and (d) show the XRD patterns of S3 ($Cu_{2-x}Se$) and S4 (the sintered-$Cu_{2-x}Se$), which matched well with the standard diffraction pattern of cubic mineral berzelianite $Cu_{2-x}Se$ (JCPDS card no. 06-0680). It is worth noting that s-$Cu_{2-x}Se$ maintained the phase consistency with $Cu_{2-x}Se$, and its steep diffraction peaks indicate the improved crystallinity after the calcination treatment.

Furthermore, the morphology and phase composition of the as-prepared copper selenide samples were characterized by SEM and TEM. Fig. 2(a) displays the SEM images of CuSe with different resolutions. It can be seen that the CuSe sample exhibits two types of morphologies, namely sphere-like and sheet-like morphologies. Thereinto, the particle sizes of the sheets are relatively large and their diameters are approximately from 2 to more than 5 μm. Respectively, the spheres are relatively smaller, with diameters ranging from about 200 to 700 nm. Different from CuSe, the particles of Cu_3Se_2 (Fig. 2(b)) are much smaller (diameters are less than 100 nm), and many of them can be recognized as wedge-like shapes, as shown in the zoomed image. Fig. 2(c) displays the SEM images of $Cu_{2-x}Se$. It can be seen that $Cu_{2-x}Se$ also consists of nanoparticles with diameters less than 100 nm, but they are mostly round shapes seen from the zoomed image. However, the particle size and morphology of $Cu_{2-x}Se$ turn out to be quite different after calcination, as shown in Fig. 2(d). Clearly, all the nanoparticles disappeared and fused into a large bulk structure. The nanoparticles fused so well that no apparent cracks can be seen in the zoomed image.

More morphological information has been provided based on the TEM characterization. Fig. 3(a) and (d) show the TEM and HRTEM images of CuSe, respectively. Clearly, larger-sized sheets and smaller-sized spherical bulks can be seen in Fig. 3(a), which is consistent with the SEM result, as shown in Fig. 2(a). HRTEM images were obtained on both the sheets and the spherical bulks, and it is interesting to note that both structures share the same lattice distance of about 0.33 nm, as shown in Fig. 3(d). This lattice distance can be identified as the lattice spacing of the (101) plane in hexagonal klockmannite CuSe,[31] indicating that the sample consists of pure CuSe with two different morphologies. TEM and HRTEM images of Cu_3Se_2 are shown in Fig. 3(b) and (e), respectively. The diameters of the nanoparticles of Cu_3Se_2 can be estimated more precisely to be about 15–30 nm from Fig. 3(b). Also, the wedge-like shapes of the nanoparticles can be recognized more clearly. Fig. 3(e) exhibits the HRTEM image of Cu_3Se_2, whereby the interplanar spacing is about 0.35 nm, which agrees well with the (101) planes of tetragonal umangite Cu_3Se_2.[32] It can be seen in Fig. 3(c) and (f) that the diameters of the nanoparticles of $Cu_{2-x}Se$ were estimated at about 10–20 nm and its interplanar spacing is about 0.33 nm, which corresponds to the (111) planes of the cubic β-phase berzelianite of $Cu_{2-x}Se$. Though our $Cu_{2-x}Se$ sample was synthesized at RT, it is confirmed to have a high-temperature β-phase structure instead of a low-temperature α-phase structure, whose interplanar spacing of the (111) planes should be doubled (about 0.66 nm) than that of the β-phase structure.[10] This can be explained by the low α–β transition temperature of $Cu_{2-x}Se$ (about 340–400 K), which is very close to RT. Moreover, the nano-sized β-phase structure $Cu_{2-x}Se$ is considered to be more thermodynamically stable and commonly fabricated below 400 K.[33] The imperfection of crystallinity of $Cu_{2-x}Se$ can also be seen in HRTEM in another resolution, as shown in the ESI (Fig. S1†).

The TE properties of the copper selenide samples, including Seebeck coefficient, electrical conductivity, and thermal conductivity, were then examined in the temperature range of 30–150 °C (about 303 to 423 K), and the *ZT* values were calculated based on these tests. The actual photos, surface SEM images, and EDX analysis results of the pressed samples are

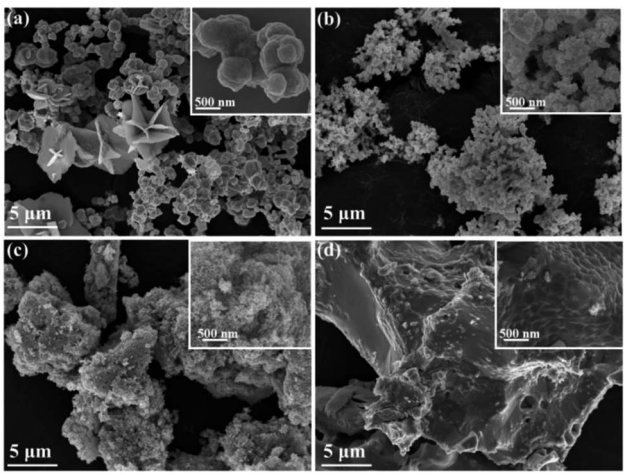

Fig. 2 SEM images of (a) CuSe, (b) Cu_3Se_2, (c) $Cu_{2-x}Se$, and (d) s-$Cu_{2-x}Se$.

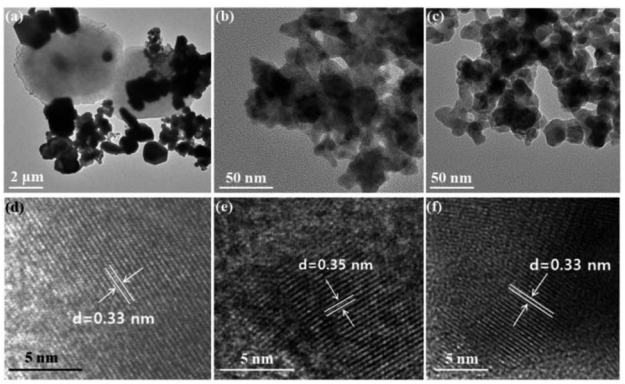

Fig. 3 TEM and HRTEM images of CuSe (a and d), Cu_3Se_2 (b and e) and $Cu_{2-x}Se$ (c and f), respectively.

shown in the ESI (Fig. S2–S4†). First, the temperature dependencies of Seebeck coefficients of the samples, are shown in Fig. 4(a). Clearly, all the as-synthesized samples possessed positive Seebeck coefficients, indicating that they are all p-type TE materials. For the as-prepared CuSe, Cu_3Se_2 and $Cu_{2-x}Se$ samples, their Seebeck coefficients are in the range of 15.3–23.3 μV K^{-1}, 17.2–29.1 μV K^{-1} and 25.8–46.6 μV K^{-1}, respectively. It can be noticed that the order of Seebeck coefficients from high to low was $Cu_{2-x}Se$ > Cu_3Se_2 > CuSe. The differences in the Seebeck coefficients resulted from different crystal structures, thus giving rise to different electron band structures and electron scattering. Moreover, the Seebeck coefficient of the sintered $Cu_{2-x}Se$ (s-$Cu_{2-x}Se$) has a slight increase compared to that of the original one, particularly above 360 K. The highest Seebeck coefficient value shown by s-$Cu_{2-x}Se$ was about 52.5 μV K^{-1} near 423 K.

Fig. 4(b) exhibits the electrical conductivity of these samples. The σ values of the three as-prepared copper selenide samples are close with each other in the measured temperature range, CuSe is about (6.1–7.6) × 10^4 S m^{-1}, Cu_3Se_2 was (7.9–8.8) × 10^4 S m^{-1} and $Cu_{2-x}Se$ was (3.64.3) × 10^4 S m^{-1}, respectively. However, after sintering, the σ value of s-$Cu_{2-x}Se$ significantly increased to about (24.4–36.3) × 10^4 S m^{-1}, which was almost 10 times higher than that of the untreated $Cu_{2-x}Se$ sample. Sintering is widely utilized for accelerating the TE performance of the materials constructed by wet-chemistry methods as the crystallinity of $Cu_{2-x}Se$ can be effectively improved after sintering.[18,21,31] This improvement can be verified by the XRD patterns, as shown in Fig. 1(c) and (d) in our study. In addition, based on the SEM images shown in Fig. 2(c) and (d), the $Cu_{2-x}Se$ nanoparticles fused densely into bulks after sintering, which leads to better electronic transportation pathways inside the material and further increase the electrical conductivity.

Thermal conductivity was examined at 303, 333, 363, 393 and 423 K, and the results are shown in Fig. 4(c). It can be seen that all the κ values of the samples are below 1.00 W m^{-1} K^{-1} in the measured temperature range, and they decrease with an increase in the temperature. The order of κ values of the three as-prepared samples from high to low is CuSe > Cu_3Se_2 > $Cu_{2-x}Se$; CuSe is about 0.84–0.99 W m^{-1} K^{-1}, Cu_3Se_2 is 0.68–0.81 W m^{-1} K^{-1}, and $Cu_{2-x}Se$ is 0.39–0.47 W m^{-1} K^{-1}. Among them, the κ value of $Cu_{2-x}Se$ is less than half of the other two samples. This result indicates that $Cu_{2-x}Se$ is the best TE material candidate among the three copper selenides with different stoichiometric compositions, which agrees with the results reported by other researchers focusing on copper selenides. The relatively low thermal conductivity of $Cu_{2-x}Se$ can be due to its unique crystal phonon-glass electron-crystal structure. In the cubic β-phase structure, the Cu ions are superionic and kinetically disordered throughout the phase structure, which can enhance the scattering of phonons and finally decrease the thermal conductivity.[10] Conversely, neither CuSe, Cu_3Se_2 nor the α-phase $Cu_{2-x}Se$ is convinced to have such liquid-like Cu ions. Besides, the imperfection of crystallinity of the as-prepared $Cu_{2-x}Se$ sample, which can be seen from the XRD (Fig. 1(c)) and HR-TEM (Fig. 3(f)) tests, also leads to its relatively low thermal conductivity. Though sintering is beneficial for obtaining better Seebeck coefficient and electrical conductivity results for the as-prepared $Cu_{2-x}Se$ sample, the κ value of s-$Cu_{2-x}Se$ unfavorably increases to about 0.62–0.74 W m^{-1} K^{-1} compared to that of the untreated one, and the TE performance is affected simultaneously. This may be ascribed to the bulk structure evolved from the nanoparticles after sintering, which is beneficial to promote the transportation of not only the electrons but also the phonons and result in an increase in both electrical and thermal conductivity.

The eventual calculated *ZT* values of the samples are shown in Fig. 4(d). All the *ZT* values of the samples increase with the increase in temperature. The *ZT* values of CuSe and Cu_3Se_2 are about 0.004–0.021 and 0.009–0.046, respectively. Owing to the higher Seebeck coefficient and lower thermal conductivity, the *ZT* values of the as-prepared $Cu_{2-x}Se$ increased slightly to 0.018–0.085 compared to that of the other two samples. After sintering, the *ZT* values of s-$Cu_{2-x}Se$ significantly increased to about 0.096–0.458. Undoubtedly, this is mainly by virtue of the enormous improvement of its electrical conductivity. This *ZT* value of s-$Cu_{2-x}Se$ is also impressive for pure copper selenide TE materials at the relatively low temperature range. The EDX analysis results (shown in Fig. S3†) reveal that the *x* values of $Cu_{2-x}Se$ and s-$Cu_{2-x}Se$ are 0.22 and 0.16, respectively. The *x* value of $Cu_{2-x}Se$ is slightly larger than the reported range ($0.15 \leq x \leq 0.2$),[34] which indicates more amounts of Cu vacancies and limits the improvement of TE performance.[30] To further improve the *ZT* values, nanostructure engineering and elemental doping are considered to be the effective strategies.[35–37]

The output voltage test of the sintered-$Cu_{2-x}Se$ sample was then investigated at 303 K. Fig. 5(a) shows the voltage–time curve of the sintered sample during heating. In the heating test, T_1 was set as the cold side and stayed at 303 K. In contrast, T_2 was set as the hot side and initially set at 303 K, followed by a successive increase of 10 K every 5 minutes with the

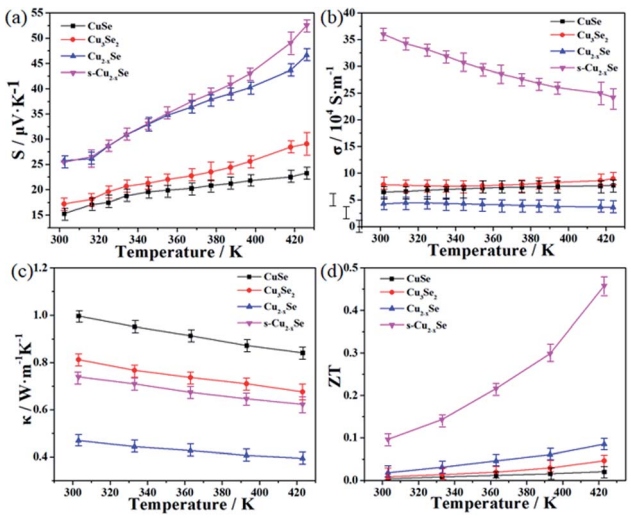

Fig. 4 Temperature dependence of Seebeck coefficients (a), electrical conductivity (b), thermal conductivity (c) and *ZT* value (d) of the samples.

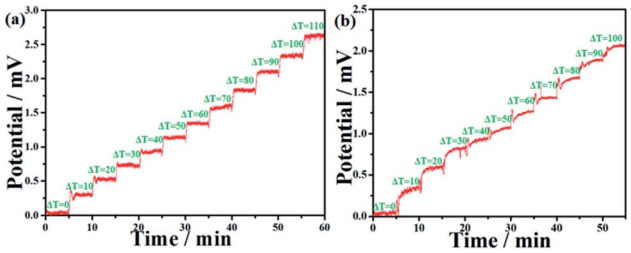

Fig. 5 *V*–*T* curves of the s-$Cu_{2-x}Se$ sample under heating (a) and cooling (b) processes, respectively.

temperature difference from 0 to 110 K. As shown in Fig. 5(a), the voltage–time curve of s-$Cu_{2-x}Se$ exhibited a well-defined step-shape, and the corresponding platforms for each temperature differences were relatively flat and stable. This result shows that the generated voltage as a function of temperature difference also exhibited excellent linearity, which is consistent with the Seebeck coefficient test and is beneficial for application in self-powered temperature sensors.[38,39]

At the cooling test of the output voltage, T_1 and T_2 were initially set at 353 K. Then, the hot side (T_2) stayed at 353 K while the cold side (T_1) successively decreased by 10 K every 5 min and eventually reached 253 K. As shown in Fig. 5(b), the cooling curve is also step-shape and increases with the increase in the temperature difference. However, the platforms are not so flat and stable compared with that of the heating curve, and the values of generated voltages are lower than that in the heating process under the same temperature difference. It may be due to the relatively slow response of the bulk sample while cooling.[40]

In addition, compared with some commonly used high-temperature synthesis methods for copper selenides which usually conduct as high as 1000 K and last about several days,[10,17,19,20] the wet chemical methods are evidently much more time- and energy-saving. It is also worth noting that the reductant sodium ascorbate for the fabrication of $Cu_{2-x}Se$, which we used here, is relatively environment-friendly and less toxic compared with other reductants such as $NaBH_4$ and $N_2H_4 \cdot 2H_2O$ that are used in other reported wet chemical methods.[18,21] Hence, herein, we provided a facile, safe and environment-friendly way to fabricate $Cu_{2-x}Se$ materials with high TE performance at a relatively low temperature range.

Conclusion

In summary, facile wet-chemistry methods were applied to the synthesis of copper selenides. XRD, SEM and TEM measurements demonstrate that copper selenides with different stoichiometric compositions, such as CuSe, Cu_3Se_2 and $Cu_{2-x}Se$, were obtained, and they differed in morphologies and sizes with each other. Among the three samples, $Cu_{2-x}Se$ exhibited the highest Seebeck coefficient and the lowest thermal conductivity, which can be attributed to its unique phonon-glass electron-crystal structure. After sintering, the $Cu_{2-x}Se$ sample attained better crystallinity and effective electronic transportation pathways, leading to a slight enhancement of the Seebeck coefficient and an enormous improvement in electrical conductivity. Though the thermal conductivity of sintered-$Cu_{2-x}Se$ rises as well, the eventual calculated *ZT* values of sintered-$Cu_{2-x}Se$ are much higher than that of the $Cu_{2-x}Se$ sample without sintering. The highest *ZT* value of sintered-$Cu_{2-x}Se$ is about 0.46 at 150 °C, which is a remarkable result for copper selenides-based TE material at a relatively low temperature range.

Conflicts of interest

There are no conflicts of interest to declare.

Acknowledgements

This work has been partially supported by the National Natural Science Foundation of China (Grant No. 52073066), the GDAS Project of Science and Technology Development (No. 2020GDASYL-20200102028, No. 2020GDASYL-20200103130, No. 2020GDASYL-20200102029 and No. 2018GDASCX-0116), and the Science and Technology Program of Guangdong Province (No. 2020B0101340005).

References

1 Y. Wang, L. Yang, X. Shi, X. Shi, L. Chen, M. S. Dargusch, J. Zou and Z. Chen, *Adv. Mater.*, 2019, **31**, 1807916.
2 D. Jiang, B. Shi, H. Ouyang, Y. Fan, Z. L. Wang and Z. Li, *ACS Nano*, 2020, **14**, 6436–6448.
3 C. Li, F. Jiang, C. Liu, P. Liu and J. Xu, *Appl. Mater. Today*, 2019, **15**, 543–557.
4 Q. Yao, Q. Wang, L. Wang and L. Chen, *Energy Environ. Sci.*, 2014, **7**, 3801–3807.
5 C. S. Kim, G. S. Lee, H. Choi, Y. J. Kim, H. M. Yang, S. H. Lim, S. G. Lee and B. J. Cho, *Appl. Energy*, 2018, **214**, 131–138.
6 P. Zong, R. Hanus, M. Dylla, Y. Tang, J. Liao, Q. Zhang, G. J. Snyder and L. Chen, *Energy Environ. Sci.*, 2017, **10**, 183–191.
7 W. Liu, L. Yang, Z. Chen and J. Zou, *Adv. Mater.*, 2020, **32**, 1905703.
8 C. Gayner and K. K. Kar, *Prog. Mater. Sci.*, 2016, **83**, 330–382.
9 T. Wei, C. Wu, F. Li and J. Li, *J. Materiomics*, 2018, **4**, 304–320.
10 H. Liu, X. Shi, F. Xu, L. Zhang, W. Zhang, L. Chen, Q. Li, C. Uher, T. Day and G. J. Snyder, *Nat. Mater.*, 2012, **11**, 422–425.
11 L. Zhao, S. Lo, Y. Zhang, H. Sun, G. Tan, C. Uher, C. Wolverton, V. P. Dravid and M. G. Kanatzidis, *Nature*, 2014, **508**, 373–377.
12 J. Fan, X. Huang, F. Liu, L. Deng and G. Chen, *Compos. Commun.*, 2021, **24**, 100612.
13 L. Zhao, S. Hao, S. Lo, C. Wu, X. Zhou, Y. Lee, H. Li, K. Biswas, T. P. Hogan, C. Uher, C. Wolverton, V. P. Dravid and M. G. Kanatzidis, *J. Am. Chem. Soc.*, 2013, **135**, 7364–7370.

14 J. Rhyee, K. H. Lee, S. M. Lee, E. Cho, S. I. Kim, E. Lee, Y. S. Kwon, J. H. Shim and G. Kotliar, *Nature*, 2009, **459**, 965–968.
15 S. Lin, W. Li, S. Li, X. Zhang, Z. Chen, Y. Xu, Y. Chen and Y. Pei, *Joule*, 2017, **1**, 816–830.
16 Y. Liu, G. García, S. Ortega, D. Cadavid, P. Palacios, J. Lu, M. Ibáñez, L. Xi, J. D. Roo, A. M. López, S. Martí-Sánchez, I. Cabezas, M. de la Mata, Z. Luo, C. Dun, O. Dobrozhan, D. L. Carroll, W. Zhang, J. Martins, M. V. Kovalenko, J. Arbiol, G. Noriega, J. Song, P. Wahnón and A. Cabot, *J. Mater. Chem. A*, 2017, **5**, 2592–2602.
17 H. Liu, X. Yuan, P. Lu, X. Shi, F. Xu, Y. He, Y. Tang, S. Bai, W. Zhang, L. Chen, Y. Lin, L. Shi, H. Lin, X. Gao, X. Zhang, H. Chi and C. Uher, *Adv. Mater.*, 2013, **25**, 6607–6612.
18 D. Li, X. Y. Qin, Y. F. Liu, C. J. Song, L. Wang, J. Zhang, H. X. Xin, G. L. Guo, T. H. Zou, G. L. Sun, B. J. Ren and X. G. Zhu, *RSC Adv.*, 2014, **4**, 8638–8644.
19 A. A. Olvera, N. A. Moroza, P. Sahoo, P. Ren, T. P. Bailey, A. A. Page, C. Uher and P. F. P. Poudeu, *Energy Environ. Sci.*, 2017, **10**, 1668–1676.
20 S. Butt, M. U. Farooq, W. Mahmood, S. Salam, M. Sultan, M. A. Basit, J. Ma, Y. Lin and C. Nan, *J. Alloys Compd.*, 2019, **786**, 557–564.
21 Q. Hu, Z. Zhu, Y. Zhang, X. Li, H. Song and Y. Zhang, *J. Mater. Chem. A*, 2018, **6**, 23417–23424.
22 W. Liao, L. Yang, J. Chen, D. Zhou, X. Qu, K. Zheng, G. Han, J. Zhou, M. Hong and Z. Chen, *Chem. Eng. J.*, 2019, **371**, 593–599.
23 J. Lei, Z. Ma, D. Zhang, Y. Chen, C. Wang, X. Yang, Z. Cheng and Y. Wang, *J. Mater. Chem. A*, 2019, **7**, 7006–7014.
24 D. Yang, X. Su, J. Li, H. Bai, S. Wang, Z. Li, H. Tang, K. Tang, T. Luo, Y. Yan, J. Wu, J. Yang, Q. Zhang, C. Uher, M. G. Kanatzidis and X. Tang, *Adv. Mater.*, 2020, **32**, 2003730.
25 Z. Lin, C. Hollar, J. S. Kang, A. Yin, Y. Wang, H. Shiu, Y. Huang, Y. Hu, Y. Zhang and X. Duan, *Adv. Mater.*, 2017, **29**, 1606662.
26 Y. Lu, Y. Ding, Y. Qiu, K. Cai, Q. Yao, H. Song, L. Tong, J. He and L. Chen, *ACS Appl. Mater. Interfaces*, 2019, **11**, 12819–12829.
27 S. Ballikaya, H. Chi, J. R. Salvadorc and C. Uher, *J. Mater. Chem. A*, 2013, **1**, 12478–12484.
28 T. Zhang, Y. Song, X. Zhang, X. He and J. Jiang, *Mater. Lett.*, 2019, **250**, 189–192.
29 L. Yang, J. Wei, Y. Qin, L. Wei, P. Song, M. Zhang, F. Yang and X. Wang, *Materials*, 2021, **14**, 2075.
30 J. Tak, W. H. Nam, C. Lee, S. Kim, Y. S. Lim, K. Ko, S. Lee, W. Seo, H. K. Cho, J. Shim and C. Park, *Chem. Mater.*, 2018, **30**, 3276–3284.
31 X. Liu, X. Duan, P. Peng and W. Zheng, *Nanoscale*, 2011, **3**, 5090–5095.
32 Q. Wang, *Mater. Lett.*, 2009, **63**, 1493–1495.
33 F. Gao, S. L. Leng, Z. Zhu, X. J. Li, X. Hu and H. Z. Song, *J. Electron. Mater.*, 2018, **47**, 2454–2460.
34 V. M. Garcia, P. K. Nair and M. T. S. Nair, *J. Cryst. Growth*, 1999, **203**, 113–124.
35 Z. Zhu, Y. Zhang, H. Song and X. Li, *Appl. Phys. A*, 2019, **125**, 572.
36 Z. Zhu, Y. Zhang, H. Song and X. Li, *Appl. Phys. A*, 2018, **124**, 871.
37 Y. Qin, L. Yang, J. Wei, S. Yang, M. Zhang, X. Wang and F. Yang, *Materials*, 2020, **13**, 5704.
38 X. Chen, Z. Ren, H. Guo, X. Cheng and H. Zhang, *Appl. Phys. Lett.*, 2020, **116**, 043902.
39 M. Li, J. Chen, W. Zhong, M. Luo, W. Wang, X. Qing, Y. Lu, Q. Liu, K. Liu, Y. Wang and D. Wang, *ACS Sens.*, 2020, **5**, 2545–2554.
40 W. Zeng, X. Tao, S. Lin, C. Lee, D. Shi, K. Lam, B. Huang, Q. Wang and Y. Zhao, *Nano Energy*, 2018, **54**, 163–174.